PCCP

Cite this: *Phys. Chem. Chem. Phys.*, 2011, **13**, 12554–12558

www.rsc.org/pccp

**PAPER**

# High performance supercapacitors based on highly conductive nitrogen-doped graphene sheets†

**Yongcai Qiu, Xinfeng Zhang and Shihe Yang***

***Received 12th April 2011, Accepted 27th April 2011***
**DOI: 10.1039/c1cp21148j**

Thermal nitridation of reduced graphene oxide sheets yields highly conductive ($\sim$1000–3000 S m$^{-1}$) N-doped graphene sheets, as a result of the restoration of the graphene network by the formation of C–N bonded groups and N-doping. Even without carbon additives, supercapacitors made of the N-doped graphene electrodes can deliver remarkable energy and power when operated at higher voltages, in the range of 0–4 V.



Supercapacitors rely on electric double-layers (EDL) for the direct, fast physical storage and release of electric energy,[1] and can thus offset the deficiencies of other power sources such as batteries and fuel cells. By virtue of their highly reversible charge storage process, supercapacitors enjoy a long cycle life and can work at high rates.[2] Given their advantages over conventional energy storage devices in terms of high power density, high reliability, light weight, convenient packaging and low maintenance,[3] supercapacitors are expected to power hybrid electric vehicles (HEV), electric vehicles (EV), load cranes, and forklifts.[1–5] However, the energy density of EDL capacitors (EDLCs) ($<$30 W h kg$^{-1}$) is significantly lower than that of rechargeable batteries ($>$100 W h kg$^{-1}$). Although pseudocapacitors made of conducting polymers or metal oxides have shown high capacitances associated with both surface and reversible Faradic redox processes,[6–8] they still suffer from the relatively short lifetimes and capacitance degradation due to the Faradic redox reactions.

Carbon materials such as activated carbon (AC) and carbon nanotubes (CNTs) are commonly used as electrode materials for EDLCs, owing to their good thermal and chemical stability and high electrical conductivity.[9] Although the commercial AC powders have high specific surface areas of 1000–3000 m$^2$ g$^{-1}$, their particulate morphology, pore size distribution and uncontrollable surface functional groups largely restrict the cycle life and power density. CNTs, particularly single-walled carbon nanotubes, have well-defined structures and high conductivities without any functional groups, and thus appear to satisfy all of the requirements for EDLCs. In spite of their superior structural and electrical properties, CNT-based supercapacitors have not delivered the expected performance, due primarily to the low specific surface area, high contact resistance between the electrode and the current collector, and adventitious chemical impurities.[9,10] For example, the preparation of CNTs requires metallic catalysts that are not easily removable. Such metallic impurities can bring about parasitic reactions that compromise device lifetimes. Vertically growing CNTs on a conductive substrate could reduce the contact resistance, but this causes problems of low volumetric capacitance and relatively high cost. Metal oxide decorated CNTs could resolve these problems by combining the high conductivity of the CNTs with the pseudocapacitance of the metal oxides; however, the fabrication is time-consuming and they are difficult to implement in real devices on a large scale.

Fortunately, the carbon family has another star—graphene—which is skyrocketing, and could take up the challenge for EDLC devices thanks to its unique morphology, superior electrical conductivity, high specific surface area of over 2600 m$^2$ g$^{-1}$, and excellent structural stability.[10–13] Recent results have shown that the specific capacitance of graphene-based supercapacitors can reach 135 F g$^{-1}$, 99 F g$^{-1}$ and 75 F g$^{-1}$ in aqueous, organic, and ionic liquid electrolytes, respectively.[14,15] However, these values are far below the theoretical EDL capacitance of 520 F g$^{-1}$, supported by the intrinsic capacitance of graphene sheets ($\sim$21 μF cm$^{-2}$) found recently,[17] a value obtainable only when the entire active surface of a graphene-based electrode can access the electrolyte. The current challenge is to develop graphene materials with single or few layers combined with less agglomeration, a tailored pore-size distribution and high electrical conductivity to optimize the supercapacitor performance.[13–16]

We report herein an effective nitrogen-doping approach to dramatically enhance the electrical conductivity of pristine graphene oxide sheets, generating nitrogen-doped graphene (NG) sheets. In this approach, care was also taken to minimize agglomeration of the graphene sheets. Significantly improved

*Nano Science and Technology Program, Department of Chemistry, William Mong Institute of Nano Science and Technology, The Hong Kong University of Science and Technology, Clear Water Bay, Kowloon, Hong Kong, China. E-mail: chsyang@ust.hk*

† Electronic supplementary information (ESI) available: Experimental Section, FT-IR, XPS, TGA and Pore Diameter Distribution. See DOI: 10.1039/c1cp21148j

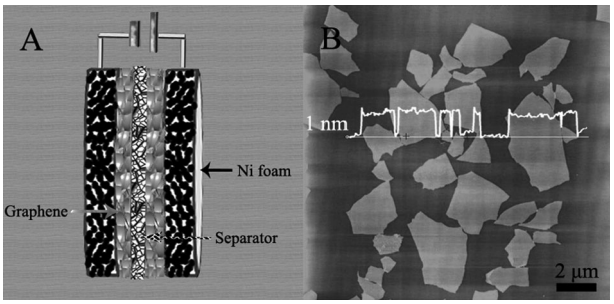


**Fig. 1** (A) A schematic representation of the graphene-based supercapacitor device. (B) A typical AFM image of the GO sheets. The white trace shows the height profile.

specific capacitances and rate capabilities have been demonstrated by supercapacitors made of these NG sheets. Fig. 1a shows the supercapacitor assembly used for testing our NG sheets, which is customarily adopted in industry (see ESI,† Experimental Section). Our approach consists of three major steps. First, the starting graphene oxide (GO) sheets were synthesized by a modification of Hummers's method.[18,19] The tapping-mode atomic force microscope (AFM) image in Fig. 1b clearly shows that the GO sheets are only one carbon layer thick. Second, the GO sheets were transformed into reduced GO (RGO) sheets by hydrazine in aqueous solution. To combat agglomeration, we resorted to sonication treatment. Finally, highly conductive NG sheets with minimal agglomeration were obtained by thermal reduction of the RGO sheets in an atmosphere of $NH_3$ gas (see the Experimental Section in the ESI†).

Graphene oxide has relatively low electrical conductivity, because the harsh oxidation in the preparation process impairs the $sp^2$ atomic network structure of graphene. Literally, graphene oxide consists of basal plane carbon atoms decorated with epoxy and hydroxyl groups and edge carbon atoms attached by carbonyl and carboxyl groups, as evidenced by XPS, Raman and FT-IR spectra (see ESI,† Figs S1, S2 and S3).[20,21] Hydrazine is a good reducing agent,[22] which has indeed converted the GO sheets to RGO sheets. In contrast, the RGO sheets contain fewer $sp^3$ carbon atoms, as revealed by XPS and FT-IR spectra (see ESI,† Figs S1 and S2). Of note, the sonication treatment has to a large degree helped to reduce the agglomeration of the RGO sheets. This can be seen from their generally curling and bendy morphology, which has been carried through to the final NG sheets, obtained after freeze-drying and thermal nitridation of the RGO sheets. In addition, a TEM image (see ESI,† Fig. S5) also reveals numerous wrinkles of the as-obtained NG sheets. These curls and wrinkles clearly act to prevent graphene sheets from restacking together with one another. The Brunauer–Emmett–Teller (BET) surface areas of the RGO and NG sheets have been measured to be 615.2 $m^2 g^{-1}$ and 630.6 $m^2 g^{-1}$, respectively. Both values, albeit much lower than the theoretical value ($\sim$2600 $m^2 g^{-1}$) of graphene sheets, are fairly high considering the strong tendency of agglomeration of the material. The surface areas are also comparable to those of graphene samples previously synthesized by other methods.[14,15,23] The pore size distributions of the RGO and NG sheets are in the range of 3–35 nm, as estimated from the Barrett–Joyner–Halenda (BJH) equation (See ESI,† Fig. S6), suggesting close packing of the curved and wrinkled nitrogen-doped graphene sheets. Pore diameters in this size range were previously demonstrated to perpetuate stable electrochemical behavior, which is important for device applications.[3,9] The similar surface areas and pore size distributions of the RGO and NG sheets are consistent with the fact that the sheet morphologies are changed little by nitridation, as revealed by SEM images (Fig. 2). Earlier, Jang *et al*. already recognized the ability of such a curved graphene sheet morphology to abate agglomeration when packed or compressed into an electrode structure, thereby largely enhancing EDL capacitance in an ionic liquid electrolyte. Owing to the relatively low conductivity ($\sim$100–300 S $m^{-1}$) of the RGO sheets, however, excess carbon additives had to be added into the thin film electrode.[23]

The most important contribution of this work is the outstanding electrical conductivity improvement of the NGs over the GOs and RGOs. Generally, carboxylic acid groups are unlikely to be reduced by hydrazine under the given reaction conditions, hence they usually remain in the reduced product, as vindicated by XPS, FT-IR and TGA analyses (see ESI,† Figs S1, S2 and S3). The pendent acidic surface functionalities in RGO are prone to high self-discharge when used in supercapacitor electrodes, and their removal should reduce the equivalent series resistance (ESR) and, consequently, raise the power density.[24,25] We have accomplished this by thermal nitridation of the RGO in $NH_3$ gas at 700 °C. Significantly, the thermal nitridation process resulted in the complete removal of the oxygenated surface functionalities, as evidenced by XPS, FT-IR and TGA analyses (see ESI,† Figs S1, S2 and S4). From the XPS result (see ESI,† Fig. S1), the resulting NG product contains only carbon and nitrogen, with a C/N elemental ratio of $\sim$98 : 2. The electrical conductibility of the NG product was determined to be as high as $\sim$1000–3000 S $m^{-1}$ (see detailed analysis in the ESI and Fig. S7), presumably due to the restoration of the graphene network by the formation of C–N bonded groups and

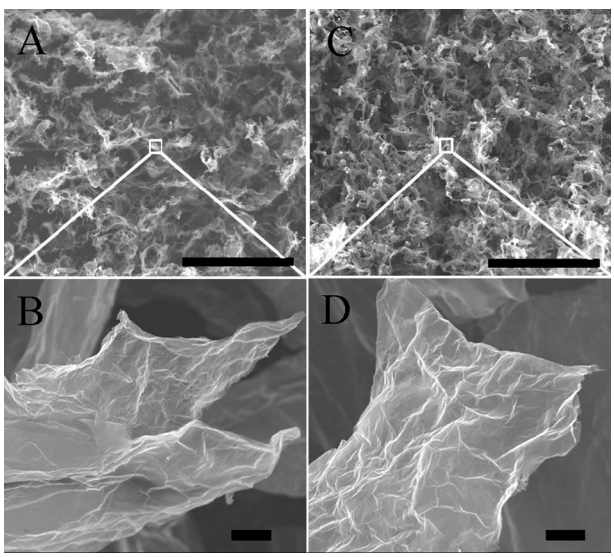


**Fig. 2** Scanning electron microscopy (SEM) images of the RGO (A, B) and NG (C, D) sheets. The enlarged SEM images (B and D) lay bare the general curling and bendy morphology of the sheets. Scale bars: 100 μm (A, C); 1 μm (B, D).

N-doping.[26–28] Another noteworthy feature of such NG sheets is their very high thermal stability—they decompose only when the temperature is above 750 °C (see ESI,† Fig. S4). This stands in sharp contrast with the much lower thermal stability (180 °C) of the RGO sheets. The latter suffers from weight loss due to the decomposition of the oxygenated surface functionalities, which could bring about high self-discharge when used for supercapacitor electrodes, and would therefore compromise device lifetimes.

Thin film electrodes of the NG sheets were fabricated together with those of the RGO sheets so as to evaluate their supercapacitor performance (see Fig. 1a and the Experimental Section in the ESI†). Note that the NG-based supercapacitor electrodes can be free of any carbon additives due to the relatively high electrical conductivity of the NG sheets. For comparison, commercial activated carbon (AC) powder with a specific surface area of $\sim$1600 $m^2$ $g^{-1}$ was also tested. Fig. 3a shows cyclical voltammograms (CVs) of the three electrodes (NG, RGO and AC) in a conventional organic solvent-based electrolyte. The curves all have a similarly symmetric trapezoid shapes. However, differences also exist. For example, the commercial AC electrode exhibits several obvious CV peaks due to parasitic chemical reactions initiated by impurities within the electrode. The CVs of the two graphene-based electrodes (NG and RGO) are nearly rectangular, indicating little contribution from faradic psedocapacitance for both supercapacitors. It should be emphasized that the operating voltage range for this organic solvent-based electrolyte can be up to 4 V, which is clearly advantageous in delivering higher energy and power densities than water-based electrolytes (1 V).[9] A higher operating voltage corresponds to a higher overall performance of the supercapacitor, as the energy and power are both proportional to the square of the voltage ($E = 1/2CV^2$ and $P_{max} = V^2/4R$, where $C$ is the cell capacitance, $V$ is the voltage and $R$ is the ESR).

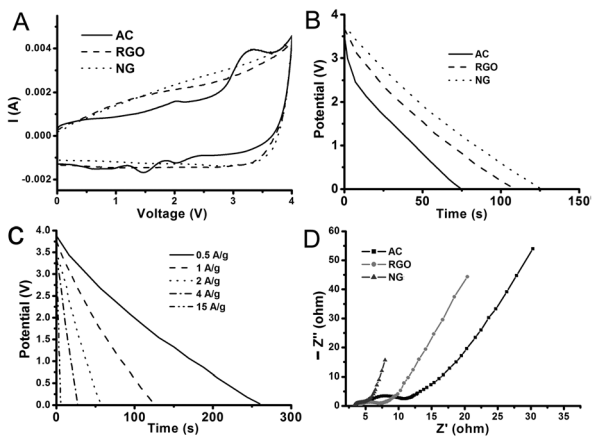


**Fig. 3** (A) Cyclic voltammograms of the AC, RGO and NG electrodes measured at 5 mV $s^{-1}$. (B) Galvanostatic discharge of the AC, RGO and NG electrodes at 1 A $g^{-1}$. (C) Galvanostatic discharge curves of the NG electrodes at various rates in the voltage range of 0–4 V, and (D) Nyquist plots for the AC, RGO and NG electrodes using a sinusoidal signal of 5 mV over a frequency range from 100 kHz to 1 mHz. $Z'$ is the real impedance and $Z''$ is the imaginary impedance.

Galvanostatic cycling of the supercapacitor electrodes was performed at various rates in the voltage range of 0–4 V. The capacitance values were calculated from the slope of the discharge curves, based on the equation of $C = I(\Delta t/\Delta V)$. As shown in Fig. 3b, the specific capacitance of the NG electrodes without any carbon additive is 138.1 F $g^{-1}$ at a current density of 1 A $g^{-1}$, which is much higher than those of the RGO (110.4 F $g^{-1}$) and AC (90.9 F $g^{-1}$) electrodes, even though the latter two electrodes were mixed with 10% carbon additive. This represents a clear demonstration that the high electrical conductivity of the NG sheets has boosted the electrochemical performance due to fast electron transport. Furthermore, the NG electrode can deliver capacitances of 144.9, 130.0, 124.9 and 99.6 F $g^{-1}$, respectively, at current densities of 0.5, 2, 4 and 15 A $g^{-1}$ (Fig. 3c). This impressive result is further confirmed by EIS measurements. Fig. 3d shows the Nyquist plots for the three supercapacitors. Each EIS plot presents an oblique line in the low frequency section, suggesting that the electrode process is under diffusion control. The slopes of the oblique lines are related to the formation rate of the electric double layers (EDL), the bigger the slope is, the faster the EDL will form.[29,30] From the EIS result, the slope of NG-based supercapacitor is clearly larger than those of the other two, affirming the former as a more ideal supercapacitor. The small semicircular shapes in the EIS plots in the high frequency region are related to the charge transfer resistance at the electrode/electrolyte interface.[29,30] Evidently, the NG-based supercapacitor acquired a semicircle of the smallest diameter, suggestive of the lowest charge transfer resistance. Finally, the ESRs can be obtained from the $x$-axis intercepts of the Nyquist plots in the high-frequency region. Again, the ESR of the NG-based supercapacitor (3.35 ohm) is smaller than those of the RGO- (3.92 ohm) and AC-based (4.84 ohm) supercapacitors. Taken together, the NG-based supercapacitor has the best capacitance characteristics needed for high energy and high power operation.

Good capacitance retention is crucial to the practical implementation of supercapacitors. Fig. 4a shows the performance of the three supercapacitors over 2000 charge–discharge cycles at 1 A $g^{-1}$. The graphene-based supercapacitors NG and RGO, particularly the former, show excellent durability, indicated by them having only small decays in capacitance, at 5.7% and 7.9%, respectively. In contrast, the AC electrode has decayed by as much as 38%. This is expected, for several reasons. First, all of the carbon-based supercapacitors, especially the NG and RGO sheets, primarily operate on the physical storage of electrical energy, which is a highly reversible process. More important, and unique to our NG-based supercapacitor, are the high porosity, high flexibility, high conductivity and high connectivity of the NG sheets arising from the N-doping assisted network restoration. These properties ensure the mechanical integrity and fast electronic conduction paths of the electrodes, and at the same time are propitious to the electrolyte permeation and to the accommodation of volumetric changes during charge–discharge processes.

Next, we look at the relationship between energy density and discharge current density in the form of a Ragone plot for our NG-based EDLCs (see Fig. 4b). Remarkable are the energy density values of 80.5, 76.7, 72.2, 69.4 and 55.3 W h $kg^{-1}$,

 

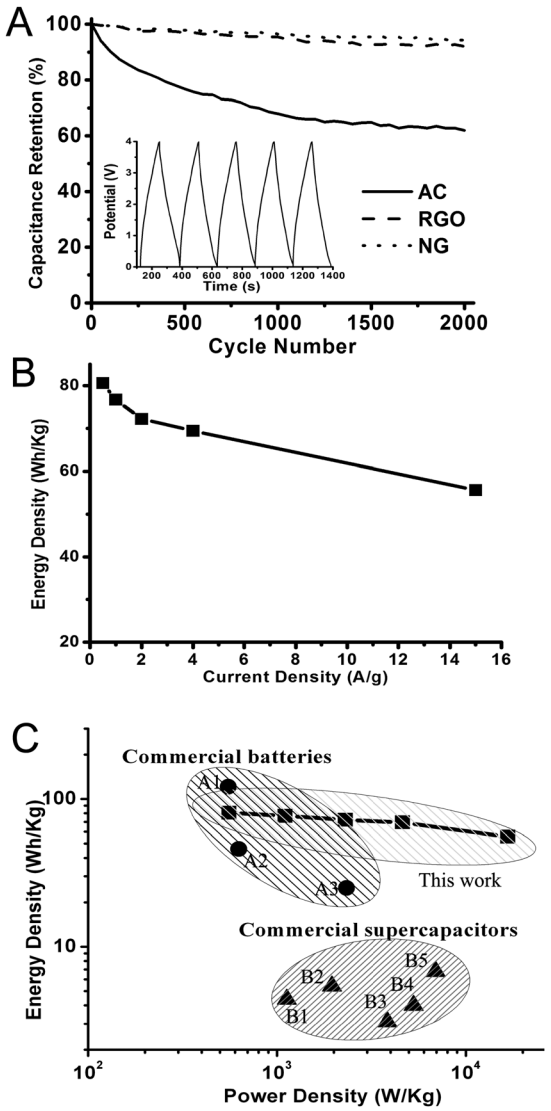


**Fig. 4** (A) Supercapacitor performance over 2000 charge–discharge cycles at 1 A $g^{-1}$. The RGO- and NG-based supercapacitors were operated at 4 V, while the AC-based supercapacitor was operated at 3 V. Inset is a galvanostatic charge–discharge curve of an NGs-based supercapacitor at 1 A $g^{-1}$. (B) The energy density of an NG-based supercapacitor as a function of discharge current density. (C) A Ragone plot (power density *vs.* energy density) of the NG-based supercapacitor and its performance in comparison with commercial batteries and supercapacitors (data taken from ref. 31. A1: Sanyo Li-ion; A2: Ovonic NiHD; A3: Bolder Pb–acid; B1: Panasonic 2000F; B2: Superfarad 250F; B3: Maxwell 1000F; B4: Maxwell 2700F; B5: Saft gen3.).

obtained at current densities of 0.5, 1, 2, 4 and 15 A $g^{-1}$, respectively. These energy densities are higher than those of the commercial NiHD (metal hydride) and Pb–acid batteries. Most importantly, the NG-based supercapacitor device can be completely recharged in minutes or even seconds. At various discharge current densities ranging from 0.5 to 15 A $g^{-1}$, the power densities are in the range of 558–16 680 W $kg^{-1}$ (Fig. 4c). It is fair to say that, in terms of energy density and power density, the performance of the NG-based supercapacitor surpasses most other carbon-based supercapacitors reported previously,[14,15,24,32–35] as well as commercial supercapacitors. The NG-based supercapacitors show a great potential for hybrid and plug-in hybrid electric vehicles (EV), backup power and others.[36–38]

In conclusion, we have significantly increased the electrical conductivity of GOs (to ~1000–3000 S $m^{-1}$) through thermal nitridation in conjunction with pre-reduction with hydrazine. The resulting curved NG sheets also display high thermal stability and are highly porous when assembled into a film. These properties result from the restoration of the graphene network by the formation of C–N bonded groups and N-doping, which are highly desirable for supercapacitors. Indeed, even without adding carbon additives into the electrodes, the NG-based supercapacitor can deliver remarkable energy and power densities operated at a high voltage of up to 4 V. Moreover, the supercapacitor has good stability, a long life and reversibility during charge–discharge cycles. In total, our results have demonstrated the great potential of N-doped curved graphene sheets as an ideal supercapacitor electrode material.

This work was supported from NSFC/HK-RGC Joint Research Scheme (N_HKUST609/09) and HK-RGC GRF (604809 and 605710).

## Notes and references


1 B. E. Conway, *Electrochemical Supercapacitors: Scientific Fundamentals and Technological Applications*, Plenum Publishers, New York, 1999.
2 M. Winter and R. J. Brodd, *Chem. Rev.*, 2004, **104**, 4245–4269.
3 R. Kötz and M. Carlen, *Electrochim. Acta*, 2000, **45**, 2483–2498.
4 A. K. Shukla, *Resonance*, 2001, **6**, 72.
5 J. R. Miller and P. Simon, *Science*, 2008, **321**, 651–652.
6 P. Simon and Y. Gogotsi, *Nat. Mater.*, 2008, **7**, 845–854.
7 H. Zhang, G. Cao, Z. Wang, Y. Yang, Z. Shi and Z. Gu, *Nano Lett.*, 2008, **8**, 2664–2668.
8 H. Wang, H. S. Casalongue, Y. Liang and H. Dai, *J. Am. Chem. Soc.*, 2010, **132**, 7472–7477.
9 A. G. Pandolfo and A. F. Hollenkamp, *J. Power Sources*, 2006, **157**, 11–27.
10 M. Pumera, *Energy Environ. Sci.*, 2011, **4**, 668.
11 K. S. Novoselov, A. K. Geim, S. V. Morozov, D. Jiang, Y. Zhang, S. V. Dubonos, I. V. Grigorieva and A. A. Firsov, *Science*, 2004, **306**, 666–669.
12 Y. C. Qiu, K. Y. Yan, S. H. Yang, L. M. Jin, H. Deng and W. S. Li, *ACS Nano*, 2010, **4**, 6515–6526.
13 J. S. Wu, W. Pisula and K. Mullen, *Chem. Rev.*, 2007, **107**, 718–747.
14 M. D. Stoller, S. Park, Y. Zhu, J. An and R. S. Ruoff, *Nano Lett.*, 2008, **8**, 3498–3502.
15 Y. Wang, Z. Q. Shi, Y. Huang, Y. F. Ma, C. Y. Wang, M. M. Chen and Y. Y. Chen, *J. Phys. Chem. C*, 2009, **113**, 13103–13107.
16 S. R. Vivekchand, S. R. Chandra, K. S. Subrahmanyam, A. Govindaraj and C. N. Rao, *J. Chem. Sci.*, 2008, **120**, 9–13.
17 J. Xia, F. Chen, J. Li and N. Tao, *Nat. Nanotechnol.*, 2009, **4**, 505–509.
18 W. S. Hummers and R. E. Offeman, *J. Am. Chem. Soc.*, 1958, **80**, 1339–1339.
19 D. C. Marcano, D. V. Kosynkin, J. M. Berlin, A. Sinitskii, Z. Sun, A. Slesarev, L. B. Alemany, W. Lu and J. M. Tour, *ACS Nano*, 2010, **4**, 4806–4814.
20 W. Gao, L. B. Alemany, L. J. Ci and P. M. Ajayan, *Nat. Chem.*, 2009, **1**, 403–408.
21 C. Hontoria-Lucas, A. J. Lopez-Peinado, J. deD. Lopez-Gonzalez, M. L. Rojas-Cervantes and R. M. Martin-Aranda, *Carbon*, 1995, **33**, 1585–1592.

22 S. Stankovich, D. A. Dikin, R. D. Piner, K. A. Kohlhaas, A. Kleinhammes, Y. Jia, Y. Wu, S. T. Nguyen and R. S. Ruoff, *Carbon*, 2007, **45**, 1558–1565.
23 C. Liu, Z. Yu, D. Neff, A. Zhamu and B. Z. Jang, *Nano Lett.*, 2010, **10**, 4863–4868.
24 T. Morimoto, K. Hiratsuka, Y. Sanada and K. Kurihara, *J. Power Sources*, 1996, **60**, 239–247.
25 C.-T. Hsieh and H. Teng, *Carbon*, 2002, **40**, 667–674.
26 X. Li, H. Wang, J. T. Robinson, H. Sanchez, G. Diankov and H. Dai, *J. Am. Chem. Soc.*, 2009, **131**, 15939–15944.
27 R. Pietrzak, *Fuel*, 2009, **88**, 1871–1877.
28 X. L. Li, X. R. Wang, L. Zhang, S. W. Lee and H. J. Dai, *Science*, 2008, **319**, 1229–1232.
29 D. Y. Qu, *J. Power Sources*, 2002, **109**, 403–411.
30 W. C. Chen, T. C. Wen and H. S. Teng, *Electrochim. Acta*, 2003, **48**, 641–649.
31 A. Burke, *J. Power Sources*, 2000, **91**, 37–50.
32 V. L. Pushparaj, M. M. Shaijumon, A. Kumar, S. Murugesan, L. Ci, R. Vajtai, R. J. Linhardt, O. Nalamasu and P. M. Ajayan, *Proc. Natl. Acad. Sci. U. S. A.*, 2007, **104**, 13574–13577.
33 L. L. Zhang, R. Zhou and X. S. Zhao, *J. Mater. Chem.*, 2010, **20**, 5983–5992.
34 Z. S. Wu, D. W. Wang, W. Ren, J. Zhao, G. Zhou, F. Li and H. M. Cheng, *Adv. Funct. Mater.*, 2010, **20**, 3595–3602.
35 Z. Fan, J. Yan, L. Zhi, Q. Zhang, T. Wei, J. Feng, M. Zhang, W. Qian and F. Wei, *Adv. Mater.*, 2010, **22**, 3723–3728.
36 M. D. Stoller and Rodney S. Ruoff, *Energy Environ. Sci.*, 2010, **3**, 1294–1301.
37 P. J. Hall, M. Mirzaeian, S. I. Fletcher, F. B. Sillars, A. J. R. Rennie, G. O. Shitta-Bey, G. Wilson, A. Cruden and R. Carter, *Energy Environ. Sci.*, 2010, **3**, 1238–1251.
38 X. Zhao, B. M. Sánchez, P. J. Dobson and P. S. Grant, *Nanoscale*, 2011, **3**, 839–855.



 